# Thermochromism in Copper(II) Halide Salts. 4. $[(C_2H_5)_2NH_2]_2CuCl_4$, Structure of the High-Temperature Phase and Physical Characterization of Its Two Phases

**Darrell R. Bloomquist, Mark R. Pressprich, and Roger D. Willett***

*Contribution from the Department of Chemistry, Washington State University, Pullman, Washington 99164.* *Received December 24, 1987*

**Abstract:** The thermochromic behavior of the title compound, bis(diethylammonium)tetrachlorocuprate(II), has been studied by a variety of techniques, including DSC, single-crystal X-ray diffraction, $^1H$ NMR, EPR, and magnetic susceptibility methods. The salt undergoes a first-order phase transition at 50 °C, changing from green to yellow with increasing temperature. The monoclinic low-temperature phase has previously been shown to contain three crystallographic independent $CuCl_4^{2-}$ ions, with varying degrees of tetrahedral distortions from planarity. The high-temperature phase is also monoclinic, $P2_1/c$, with $a$ = 25.055 (9) Å, $b$ = 10.531 (5) Å, $c$ = 13.455 (5) Å, and $\beta$ = 100.63 (3)°, with $Z$ = 8. Two crystallographic independent $CuCl_4^{2-}$ ions exist in this phase, both of which have a pronounced tetrahedral distortion. Although both anions exhibit large librational motions, one is much more librationally disordered than the other. DSC results give $\Delta H_{tr}$ = 14.6 kJ/mol and $\Delta S_{tr}$ = 45 J/(mol·deg). This $\Delta S$ value corroborates the X-ray results that both anion and cation disorder as well as lattice rearrangement effects are large. The second moment of the proton NMR line decreases by 50% at $T_{tr}$, showing that the disorder of the cations is dynamic. The EPR signal of the low-temperature phase is strongly exchanged narrowed, presumably through hydrogen bonding superexchange pathways. The line width broadens drastically at $T_{tr}$, indicating that the hydrogen bonding becomes weaker. The phase transition, as in other similar salts, appears to be driven by the entropy associated with the disorder of the cations. In the low-temperature phase, strong hydrogen bonding withdraws electron density from the chloride ions, allowing the $CuCl_4^{2-}$ anions to assume geometries intermediate between square planar and tetrahedral. With increasing temperature, dynamic disorder of the cations weakens the hydrogen bonding, causing Cl-Cl electrostatic repulsions to distort the $CuCl_4^{2-}$ ions further toward a tetrahedral geometry. The discontinuous change in anion geometry accounts for the thermochromic nature of the solid-solid phase transition.

Thermochromism, which involves the change in color upon thermal stress, occurs in a wide range of materials, both organic[1] and inorganic,[2] both in solids[1,2] and in liquids,[3] and involving emission[4] as well as absorption. Two types of thermochromism are generally distinguished: continuous, involving the gradual change in band position and/or absorption edge as temperature is changed,[5] and discontinuous, where the material undergoes a phase transition.[2] In inorganic systems, these transitions are associated with a change in the coordination geometry[6] or in the effective ligand field strength of a coordinated ligand.[7] Thus the study of these phase transitions provides an excellent opportunity to investigate the factors that effect the properties of the compounds without having to make any changes, no matter how subtle, in the chemical system itself. Our studies have focused primarily on copper(II) halide systems[8-12] where the observed geometry of the chromophore is a delicate balance between crystal field stabilization energies, ligand-ligand repulsions, ionic and/or hydrogen bonding interations with counterions, and the ever ubiquitous crystal packing forces.

Perhaps the most striking example of thermochromism among inorganic compounds is provided by the compound bis(diethylammonium)tetrachlorocuprate(II) [abbreviated $(DEA)_2CuCl_4$]. At room temperature, $(DEA)_2CuCl_4$ is bright green and changes discontinuously to bright yellow at the phase transition temperature. Several studies of $(DEA)_2CuCl_4$ have been published or communicated, including optical spectroscopy,[8] magnetic,[12] and a room temperature structural investigation.[13]

In 1977, Harlow and Simonsen presented the crystal structure of the room temperature phase of $(DEA)_2CuCl_4$.[13] The compound crystallizes as green needles in the space group $P2_1/n$ with $a$ = 7.362 Å, $b$ = 15.025 Å, $c$ = 45.193 Å, $\beta$ = 89.94°, and $Z$ = 12 corresponding to a density of 1.409 g/cm$^3$. One asymmetric unit of the structure contains three tetrahedrally distorted square-planar $CuCl_4^{2-}$ ions for a total of 12 isolated copper centers in the unusually large unit cell. An ORTEP drawing of one-half of the unit cell is shown in Figure 1. The structure contains a strong subcell/supercell relation, with all reflections with $l \neq 3n$ being much weaker than those reflections with $l = 3n$. This is recognizable in Figure 1, where the three independent $CuCl_4^{2-}$ anions are equally spaced in the $z$ direction. The anions have nearly $D_{2d}$ symmetry with average trans angles of 145.3 (4)°, 159.3 (5)°, and 178.5 (7)°; average cis angles of 95.1 (1)°, 91.9 (1)°, and 90.0 (2)°; and average, librationally uncorrected bond lengths of 2.243 (2), 2.254 (1), and 2.261 (1) Å. Esd's given here correspond to actual variations in structure rather than to experimental error; anions with perfect $D_{2d}$ symmetry would have zero esd's (ignoring librational effects). All of the DEA cations are involved in a strong, two-dimensional N-H···Cl hydrogen bonding net, parallel to the $b$-$c$ plane, which stabilizes the copper coordination geometry close to square planar. Two Cl···H-N-H···Cl pathways link each pair of anions within the net. The shortest interaction is N-H···Cl = 2.297 Å (N···Cl = 3.190 Å). It is difficult to understand why nature insists on the complex low-temperature structure, but it certainly arises from a delicate balance of hydrogen bonding and

(1) Day, J. H. *Chem. Rev.* **1963**, *63*, 65.
(2) Bloomquist, D. R., Willett, R. D. *Coord. Chem. Rev.* **1982**, *47*, 125.
(3) Blank, E. W. *J. Chem. Educ.* **1945**, *20*, 171. Ouchi, A.; Takeuchi, T.; Taminaga, I. *Bull. Chem. Soc. Jpn.* **1970**, *43*, 2609. Iwasaki, V. N.; Sone, K.; Fukuda, Y. *Z. Anorg. Allg. Chem.* **1975**, *412*, 170.
(4) Hardt, H. D.; Pierre, A. *Inorg. Chim. Acta* **1977**, *25*, L59.
(5) Radjaipour, M.; Oelkrug, D. *Ber. Bunsenges. Phys. Chem.* **1979**, *82*, 159. Lever, A. P. B.; Mantovani, E.; Donini, J. C. *Inorg. Chem.* **1971**, *10*, 2424.
(6) Marcotrigiano, .; Menabue, L.; Pellacani, G. C. *Inorg. Chem.* **1976**, *15*, 2333.
(7) Fabrizzi, L.; Michelani, M.; Paoletti, P. *Inorg. Chem.* **1974**, *13*, 3019.
(8) Willett, R. D.; Haugen, J. A.; Lebsack, J.; Morrey, J. *Inorg. Chem.* **1974**, *13*, 2510.
(9) Bloomquist, D. R.; Willett, R. D.; Dodgen, H. W. *J. Am. Chem. Soc.* **1981**, *103*, 2610.
(10) Roberts, S. A.; Bloomquist, D. R.; Willett, R. D.; Dodgen, H. W. *J. Am. Chem. Soc.* **1981**, *103*, 2603.
(11) Bloomquist, D. R.; Willett, R. D. *J. Am. Chem. Soc.* **1981**, *103*, 2615.
(12) Landee, C. P.; Roberts, S. A.; Willett, R. D. *J. Chem. Phys.* **1978**, *68*, 4574.
(13) Simonsen, S. H.; Harlow, R. L. *Am. Cryst. Assoc. Ser. 2* **1977**, *5*, No. 1, Abstract HN5.

0002-7863/88/1510-7391$01.50/0 

**Table I.** Selected Metal Halide Compounds with Phase Transitions

| compound | $T_{trans}$ (°C) | $\Delta H_{trans}$ kJ/mol | $\Delta S_{trans}$ J/(mol·deg) | $T_{melt}$ (°C) | $\Delta H_{melt}$ kJ/mol | ref |
|---|---|---|---|---|---|---|
| $(CH_3)_2CHNH_3CuCl_3$ | 85 (2) | 5.8 (9) | 16 (2) | 180 (5) | 27 (1) | 10 |
| $(CH_3)_2CHNH_3CuBr_3$ | 78 (2), 100 (2) | 5.4 (9), 3.3 (9) | 15 (2), 9 (2) | | 143 (2)[b] | 24 (1) |
| $[(CH_3)_2CHNH_3)]_2CuCl_4$ | 50 (1)[a] | 12.1 (5) | 37 (1) | 155 (5) | 27 (1) | 9 |
| $(DEA)_2CuCl_4$ | 50 (1)[a] | 14.6 (9) | 45 (3) | 83 (2) | 24.1 | this work |
| | 54 | 14.7 | 44.9 | 86 | 21.6 | 20 |
| $(DEA)_2CuBr_4$ | 38 (2)[b] | | | 85 (3)[b] | | |
| $(DEA)_2ZnCl_4 \cdot H_2O$ | 60 (2)[b] | | | 90 (5)[b] | | 19 |
| | 57 | 2.4 | 7.3 | 89 | 16.7 | 20 |
| $(DEA)_2ZnCl_4 \cdot xH_2O$[c] | 25 (5) | 5.8 (9) | 19.1 | 68 (5)[d] | 19 (2) | 19 |
| $(DEA)_2CoCl_4$ | 57 | 2.3 | 7.1 | 88 | 16.7 | 20 |
| $(DEA)_2MnCl_4$ | 54 | 6.6 | 20.1 | 76 | 16.6 | 20 |

[a] Temperature at which discontinuity appears in NMR on repeated scans through the transition. [b] Temperature taken from DTA. [c] Data for partially dehydrated salt ($0.75 > x > 0$). [d] Temperature taken as peak of DSC endotherm due to extreme broadness of peak. [e] Bloomquist, D. R. Ph.D. Thesis, Washington State University, 1980.

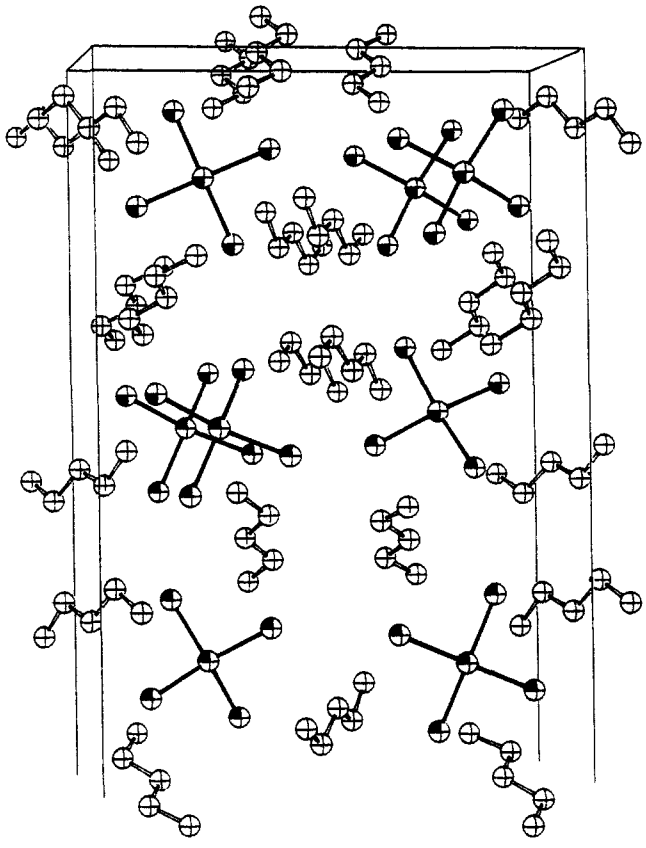

**Figure 1.** An ORTEP drawing of one-half of the unit cell of the room temperature structure of $(DEA)_2CuCl_4$ viewed normal to the *bc* plane.

crystal packing interactions. Indeed, it is easy to visualize a possible solid–solid phase transition in which the *c*-axis length decreases from 45 to 15 Å with the three independent $CuCl_4^{2-}$ anions assuming crystallographic (geometrical) equivalence.

The electronic spectrum of the room temperature phase of $(DEA)_2CuCl_4$ exhibits a broad absorption band in the d–d region centered at ~11 500 $cm^{-1}$. This band resolves into three bands at 9900, 12 900, and 15 300 $cm^{-1}$ at 9 K. In the high-temperature phase, the absorption has red shifted substantially (and discontinuously) to 7300 and 10 200 $cm^{-1}$.[8] Since the position of the absorption maximum for the d–d transitions has been correlated with the tetrahedral distortion of the $CuCl_4^{2-}$ chromophore, this gives irrefutable evidence of a change in coordination geometry for the copper(II) ion during the phase transition. From the experimental correlations, an average trans Cl–Cu–Cl angle of 135 (5)° is predicted for the $CuCl_4^{2-}$ anion. The coordination geometry so defined is in the range generally associated with the existence of only weak cation–chloride hydrogen bonding.

In this paper, the results of the investigation of the high-temperature structure and of the physical properties associated with the phase transition in $(DEA)_2CuCl_4$ are reported. Although the structure of the high-temperature phase is quite complex, a number of interesting aspects of the phase transition are brought forth. In particular, it will be shown that the intuitive feeling for the "logical" structural transition described above is wrong, and a much more complex phase transition occurs.

## Experimental Section

$(DEA)_2CuCl_4$ grows as bright green needles upon slow evaporation from an ethanol or propanol solution containing stoichiometric amounts of the amine hydrochloride and cupric chloride dihydrate. The compound can also be prepared as a pure powder by rapidly adding a large portion of diethyl ether to a saturated ethanol solution. A sample of N-deuteriated $(DEA)_2CuCl_4$ (abbreviated $(d\text{-}DEA)_2CuCl_4$) was prepared by successive recrystallization from $D_2O$. The sample was purified by adding dry ether to a saturated solution of $(d\text{-}DEA)_2CuCl_4$ in deuteriated ethanol followed by filtration in a dry nitrogen atmosphere. Heating the material for any extended period of time leads to the formation of a red substance which analyzes as $(DEA)_4Cu_4Cl_{10}O$ which contains the $Cu_4Cl_{10}O^{4-}$ cluster anion.[14] The compounds are somewhat hygroscopic but are stable indefinitely when stored under a desiccant.

A DTA scan run on a pure sample with a scan rate of 10 deg/min shows a sharp endotherm at the transition temperature (50 °C) and a sharp melting point at 83 °C. The phase transition temperature is affected by sample purity, particle size, previous history, and even relative humidity, making it difficult to define a precise transition temperature. Similar behavior was observed for $[(CH_3)_2CHNH_3]_2CuCl_4$. Thermodynamic data have been obtained by integration of the DSC endotherm measured with a scan rate of 5 deg/min. These are tabulated in Table I, along with results for other related compounds.

In order to obtain X-ray data for the high-temperature phase, a single crystal grown above the transition temperature (50 °C) was sought since warming a crystal of the low-temperature phase through the transition invariably leads to loss of crystallinity. Attempts to grow crystals from a hot (~70 °C) aqueous or ethanol solution were unsuccessful. Since the compound does not rapidly decompose to the oxide at temperatures near the melting point, crystals of the high-temperature phase can be grown from the melt. A sample of twice-recrystallized, dehydrated, and powdered $(DEA)_2CuCl_4$ was almost entirely melted on a glass slide in a hot stage. The small amount of unmelted solid provided numerous nucleation sites upon cooling. The process was repeated in order to eliminate much of the polycrystallinity of the solid. It was noted that the flat yellow crystals (principal faces (001), (00$\bar{1}$)) grown in this manner developed a reddish tint typical of $(DEA)_4Cu_4Cl_{10}O$, dependent on the time spent in the melt. Hence, the time in the melt was kept under ~3 min. A single crystal was selected with a polarizing microscope and placed in a capillary in preparation for data collection. The above steps were carried out in a partially open box (~1 m × 0.5 m × 0.5 m) heated as warm as the worker could tolerate (~55 °C) in order to avoid the first order, crystal destroying phase transition. The crystal, enclosed in the capillary, was then rapidly transferred to the diffractometer. A heating device attached to the $\chi$-circle and directing warm air along the $\phi$ axis maintained the crystal at 60.5 (5) °C for the 5-day data-collection period. X-ray diffraction data were collected on a Syntex $P2_1$ diffractometer (upgraded to Nicolet P3F specifications) with use of graphite monochromated Mo K$\alpha$ radiation.[15] The crystal was determined to belong to Laue group $2/m$ and a quarter of the sphere of reflection ($h$ and $k \geq 0$,

(14) Harlow, R. L.; Simonsen, S. H. *Am. Cryst. Assoc. Ser. 2* **1976**, *4*, No. 2, Abstract PB10.

(15) Campana, C. F.; Shepard, D. F.; Litchman, W. M. *Inorg. Chem.* **1981**, *20*, 4039.

**Table II.** $(C_4H_{12}N)_2CuCl_4$ Crystal Data (High-Temperature Phase)

| | |
|---|---|
| crystal dimens | 0.33 × 0.50 × 0.08 mm$^3$ |
| formula wt | 353.68 |
| *a* | 25.055 (9) Å |
| *b* | 10.531 (5) Å |
| *c* | 13.455 (5) Å |
| $\beta$ | 100.63 (3)° |
| vol | 3489 (3) Å$^3$ |
| cryst syst | monoclinic |
| space group | $P2_1/c$ (*b*-axis unique) |
| *Z* | 8 |
| $\rho$(calcd) | 1.35 g cm$^{-3}$ |
| radiation[a] | Mo K$\alpha$ |
| *F*(000) | 1464 |
| abs coeff | 18.5 cm$^{-1}$ |
| secondary extinction coeff | none |
| transmission factors | 0.990–0.798 |
| temp | 60.5 (5) °C |
| scan speed | 2.0–29.3 deg min$^{-1}$ |
| scan type | $\omega$ |
| scan range | 1.0 deg |
| standards monitored/reflctns | 2/100 |
| standard reflctns | 1,1,5;2,0,6 |
| reflctns collected | 3687 |
| unique reflctns | 3252 |
| *R* for equivalent reflctns | 0.0261 |
| unique reflctns with $F_o > 3\sigma$ | 1942 |
| weighting factor, $g$[b] | 0.00162 |
| $R(F)$[c] ($F \geq 3\sigma(F)$) | 0.0873 |
| $R_w(F)$[d] ($F \geq 3\sigma(F)$) | 0.0953 |
| $R(F)$[c] (all unique, allowed reflctns) | 0.1353 |
| $R_w(F)$[d] (all unique, allowed reflctns) | 0.1031 |
| goodness of fit | 1.513 |
| highest peak on final diff map | 0.86 e/Å$^3$, 2.13 Å from Cl(6) |
| no. of parameters | 266 |
| final mean parameter shift/$\sigma$ | 0.005 |

[a] Graphite monochromated. [b] $w = 1/[\sigma^2(F) + g^*F^2]$. [c] $R = \sum||F_o| - |F_c||/\sum|F_o|$. [d] $R_w = [\sum w(|F_o| - |F_c|)^2/\sum w|F_o|^2]^{1/2}$.

all *l*) was collected with use of an $\omega$-scan technique over a range of 3–40° in $2\theta$. Little intensity was observed for $2\theta \geq 30°$. Two standards measured every 100 reflections allowed for a correction corresponding to a 10% decrease in intensity. Accurate unit cell parameters were obtained through centering of 25 reflections with $2\theta$ values between 25° and 29°. Pertinent crystallographic parameters are included in Table II.

The crystal structure was solved and refined with Nicolet SHELXTL version 5.1 (1985) programs.[16] Empirical absorption corrections were made assuming a laminar crystal. The space group $P2_1/c$ was unambiguously chosen from systematic extinctions. Initial copper and chlorine positions were taken from an earlier attempt in solving the structure in which the direct methods program MULTAN[16] was employed. Further non-hydrogen atoms were located by unsharpened Fourier difference techniques. All non-hydrogen atoms were refined anisotropically. A refinement was also completed in which carbon atoms were left isotropic ($R_W$(isotropic) = 0.1116, 186 parameters), but Hamilton's *R*-ratio test[17] rejected this hypothesis at the 0.005 significance level. A further question involved the substantial disorder of the second $(CuCl_4)^{2-}$ anion (see Figure 7), and whether the best refinement would involve resolution of statically disordered positions for any or all of the atoms in the anion. A Fourier difference map was examined in which all atoms in the anion except the atom with the most anisotropic thermal parameter Cl(8) were included. Only a single maximum was located corresponding to Cl(8) and so all atoms were assigned a single location in subsequent refinements. Hydrogen atoms were constrained to C–H and N–H bond distances of 0.96 Å with isotropic thermal parameters fixed at approximately 1.2 times the corresponding heavier atom thermal parameter. Atomic coordinates and thermal parameters are given in Table III. Angles and uncorrected bond lengths as well as librationally corrected anion bond lengths are given in Table IV. No uncertainties are given for the librationally corrected bond lengths since errors arise both from uncertainties in atomic positions and also from assumptions inherent in fitting the atomic temperature factors to a rigid body model (see also comments in the Results section). Consequently, no satisfactory error analysis has yet been done. Complete listings of hydrogen atom positions and anisotropic thermal parameters as well as a tabulation of $|F_o|$ and $|F_c|$ values have been deposited.

Measurements of the $^1$H NMR spectra of solid samples of $(DEA)_2CuCl_4$ were made with an apparatus described previously.[10] The second moment was measured as a function of temperature for both $(d\text{-DEA})_2CuCl_4$ and $(DEA)_2CuCl_4$, as shown in Figure 2. The second moment shows a slight linear decrease as the temperature is raised. Examples of the derivative spectra obtained below and above the transition temperature for $(d\text{-DEA})_2CuCl_4$ are shown in Figure 3. The integrated absorption line shape is drawn as a solid line. All of the spectra show a symmetric line shape with a narrow spike at the center

**Table III.** Atomic Coordinates (×10$^4$) and Isotropic Thermal Parameters (10$^3$ Å$^2$) for the High-Temperature Phase of $[(C_2H_5)_2NH_2]_2CuCl_4$

| | | | | |
|---|---|---|---|---|
| Cu(1) | 6252 (1) | 5210 (2) | 8362 (1) | 78 (1)* |
| Cu(2) | 8732 (1) | 9606 (2) | 1122 (2) | 114 (1)* |
| Cl(1) | 5808 (2) | 7042 (4) | 8424 (4) | 135 (2)* |
| Cl(2) | 7083 (2) | 6073 (4) | 8523 (3) | 101 (2)* |
| Cl(3) | 6499 (2) | 3479 (5) | 9261 (4) | 151 (3)* |
| Cl(4) | 5656 (2) | 4292 (4) | 7122 (3) | 112 (2)* |
| Cl(5) | 8218 (2) | 8802 (5) | 2149 (4) | 128 (2)* |
| Cl(6) | 9583 (3) | 9349 (9) | 924 (6) | 249 (5)* |
| Cl(7) | 8793 (4) | 11503 (7) | 1756 (7) | 306 (7)* |
| Cl(8) | 8383 (3) | 8387 (12) | −164 (6) | 331 (7)* |
| N(1) | 4652 (5) | 8428 (13) | 1893 (9) | 104 (6)* |
| N(2) | 2124 (6) | 6293 (13) | 1664 (10) | 143 (8)* |
| N(3) | 2843 (5) | 2775 (11) | 4442 (10) | 113 (7)* |
| N(4) | 560 (8) | 1599 (17) | 1394 (14) | 170 (11)* |
| C(1) | 4280 (10) | 9303 (23) | 3282 (21) | 199 (17)* |
| C(2) | 4262 (10) | 9343 (22) | 2237 (20) | 159 (14)* |
| C(3) | 4677 (9) | 8517 (22) | 895 (15) | 160 (13)* |
| C(4) | 5075 (11) | 7610 (28) | 625 (18) | 239 (22)* |
| C(5) | 1483 (15) | 5801 (45) | 334 (29) | 456 (42)* |
| C(6) | 1788 (11) | 6536 (34) | 723 (21) | 246 (23)* |
| C(7) | 2396 (13) | 7446 (26) | 2117 (22) | 230 (20)* |
| C(8) | 2748 (11) | 7168 (24) | 3090 (23) | 244 (23)* |
| C(9) | 2711 (12) | 892 (22) | 3450 (22) | 238 (21)* |
| C(10) | 3049 (10) | 1895 (25) | 3770 (13) | 190 (16)* |
| C(11) | 3198 (8) | 3898 (17) | 4690 (17) | 172 (12)* |
| C(12) | 2980 (10) | 4800 (24) | 5224 (22) | 303 (21)* |
| C(13) | 123 (19) | 3483 (32) | 649 (30) | 434 (43)* |
| C(14) | 293 (12) | 2766 (26) | 1426 (26) | 247 (21)* |
| C(15) | 783 (12) | 976 (30) | 2299 (27) | 213 (21)* |
| C(16) | 1050 (15) | −57 (31) | 2280 (34) | 338 (33)* |

**Table IV.** Bond Lengths (Å) and Bond Angles (deg) for the High-Temperature Phase of $[(C_2H_5)_2NH_2]_2CuCl_4$

(a) Bond Lengths (Å)

| | uncorrected | librationally corrected | | |
|---|---|---|---|---|
| Cu(1)–Cl(1) | 2.237 (5) | 2.277 | N(3)–C(10) | 1.455 (30) |
| Cu(1)–Cl(2) | 2.245 (4) | 2.276 | N(3)–C(11) | 1.481 (21) |
| Cu(1)–Cl(3) | 2.211 (6) | 2.253 | N(4)–C(14) | 1.404 (34) |
| Cu(1)–Cl(4) | 2.244 (4) | 2.267 | N(4)–C(15) | 1.406 (38) |
| Cu(2)–Cl(5) | 2.223 (6) | 2.282 | C(1)–C(2) | 1.399 (40) |
| Cu(2)–Cl(6) | 2.213 (7) | 2.278 | C(3)–C(4) | 1.474 (38) |
| Cu(2)–Cl(7) | 2.166 (8) | 2.294 | C(5)–C(6) | 1.143 (52) |
| Cu(2)–Cl(8) | 2.202 (10) | 2.320 | C(7)–C(8) | 1.467 (39) |
| N(1)–C(2) | 1.504 (29) | | C(9)–C(10) | 1.373 (36) |
| N(1)–C(3) | 1.359 (25) | | C(11)–C(12) | 1.364 (35) |
| N(2)–C(6) | 1.409 (29) | | C(13)–C(14) | 1.295 (48) |
| N(2)–C(7) | 1.469 (30) | | C(15)–C(16) | 1.279 (47) |

(b) Bond Angles (deg)

| | | | |
|---|---|---|---|
| Cl(1)–Cu(1)–Cl(2) | 96.1 (2) | C(2)–N(1)–C(3) | 114.3 (16) |
| Cl(1)–Cu(1)–Cl(3) | 141.4 (2) | C(6)–N(2)–C(7) | 112.2 (20) |
| Cl(2)–Cu(1)–Cl(3) | 96.9 (2) | C(10)–N(3)–C(11) | 112.4 (16) |
| Cl(1)–Cu(1)–Cl(4) | 97.6 (2) | C(14)–N(4)–C(15) | 119.8 (24) |
| Cl(2)–Cu(1)–Cl(4) | 136.4 (2) | N(1)–C(2)–C(1) | 112.8 (19) |
| Cl(3)–Cu(1)–Cl(4) | 97.6 (2) | N(1)–C(3)–C(4) | 110.8 (18) |
| Cl(5)–Cu(2)–Cl(6) | 135.2 (3) | N(2)–C(6)–C(5) | 121.7 (35) |
| Cl(5)–Cu(2)–Cl(7) | 96.5 (3) | N(2)–C(7)–C(8) | 111.2 (21) |
| Cl(6)–Cu(2)–Cl(7) | 99.2 (4) | N(3)–C(10)–C(9) | 114.5 (23) |
| Cl(5)–Cu(2)–Cl(8) | 94.3 (3) | N(3)–C(11)–C(12) | 113.1 (18) |
| Cl(6)–Cu(2)–Cl(8) | 94.9 (3) | N(4)–C(14)–C(13) | 125.0 (33) |
| Cl(7)–Cu(2)–Cl(8) | 146.7 (4) | N(4)–C(15)–C(16) | 120.4 (35) |

(16) Sheldrick, G. SHELXTL; Nicolet Analytical Instruments: Madison, WI, 1985.
(17) Main, P., MULTAN 78, 1978.
(18) Hamilton, W. C. *Acta Crystallogr.*, **1965**, *18*, 502.

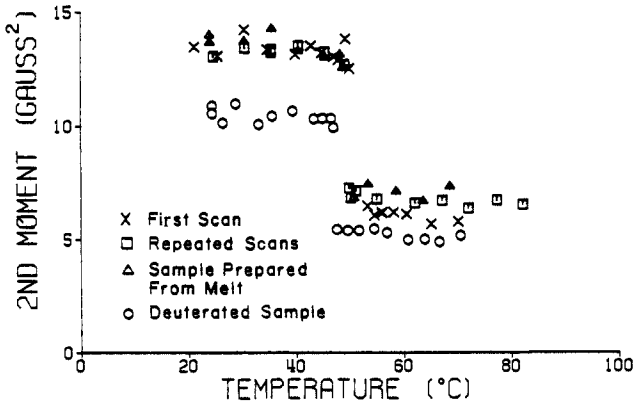


**Figure 2.** A plot of NMR second moment versus temperature for $(DEA)_2CuCl_4$ and $(d\text{-}DEA)_2CuCl_4$ showing a discontinuity at the phase transition temperature.

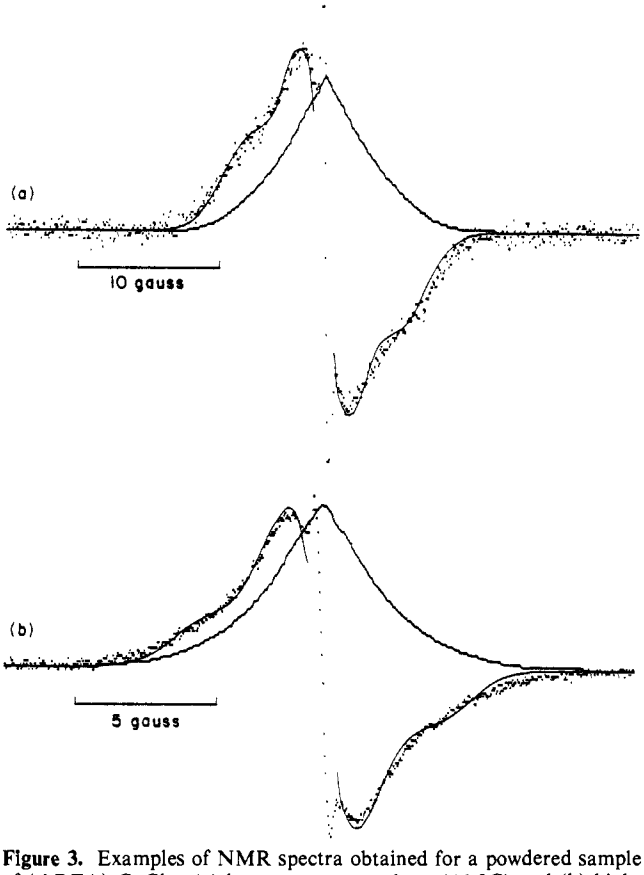


**Figure 3.** Examples of NMR spectra obtained for a powdered sample of $(d\text{-}DEA)_2CuCl_4$: (a) low-temperature phase (46 °C) and (b) high-temperature phase (50 °C). The integrated line shape and the computer fit are drawn as solid lines. Note difference in scales.

of the resonance. The narrow spike has an integrated intensity that is vanishingly small compared to the integrated intensity of the entire spectrum. This narrow resonance is assumed to be due to moisture in the sample in that its intensity can be diminished by drying in a vacuum desiccator.

With use of a Varian E-3 spectrometer equipped with a liquid circulation system, the temperature dependence of the EPR spectrum has been studied near the phase transition for both single crystal and finely powdered samples. Below the transition, an axially symmetric spectrum is observed, while above the transition temperature, a single, nearly symmetric, broad line is obtained with a peak-to-peak line width of 400 G at 55 °C. For a single crystal of the green, low-temperature phase mounted with the field perpendicular to the needle axis, a single narrow line is observed. The temperature dependence of the peak-to-peak derivative line width is plotted versus temperature in Figure 4.

Magnetic data have been obtained on a PAR vibrating sample magnetometer for the high-temperature phase of $(DEA)_2CuCl_4$ by heating a 938-mg sample to 70 °C followed by rapid quenching to the liquid-

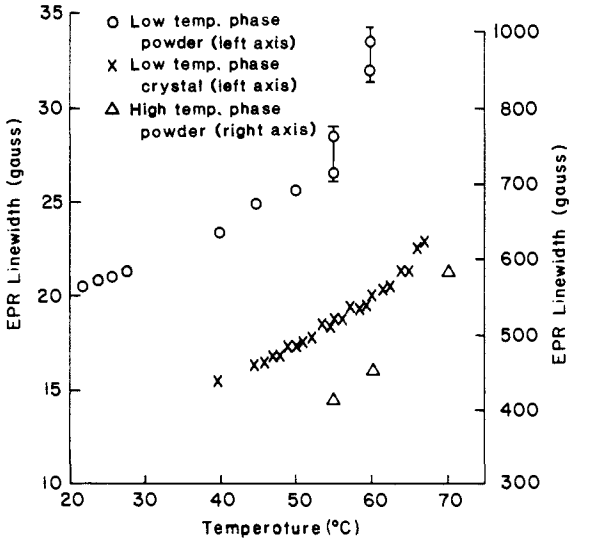


**Figure 4.** the temperature dependence of the EPR line width of a powdered sample and a single crystal of $(DEA)_2CuCl_4$. Showing line broadening prior to the phase transition. Data points drawn with error bars represent a portion of the powdered sample that super-heated after the bulk of the sample passes through the transition. The single crystal also superheated by about 15 °C. The temperature dependence of the broad line seen in the high-temperature phase is plotted against the right-hand axis.

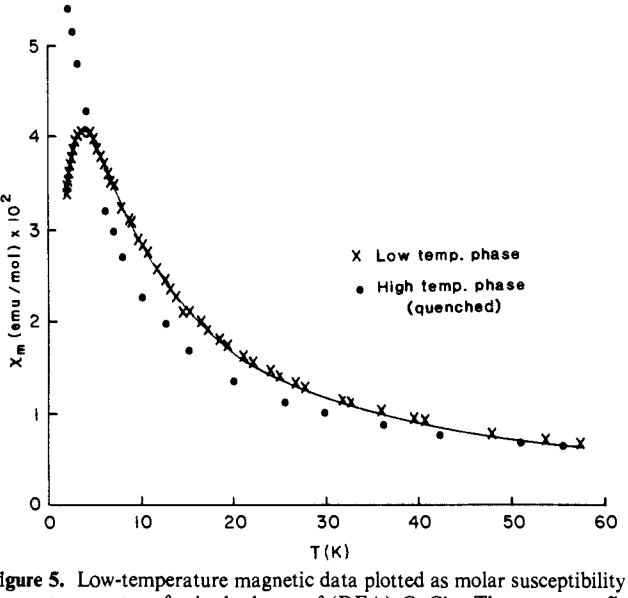


**Figure 5.** Low-temperature magnetic data plotted as molar susceptibility versus temperature for both phases of $(DEA)_2CuCl_4$. The computer fit to an antiferromagnetic two-dimensional Heisenberg model ($|J|/k$ = 1.87 K) for the low-temperature phase is drawn as a solid line.

helium temperature. Magnetic susceptibility data were collected from 2 to 250 K, at which point the transformation back to the more stable low-temperature phase occurred. All measurements were corrected for diamagnetic contributions ($-2.10 \times 10^{-4}$ emu/mol) and for temperature-independent paramagnetism of the copper ($6.00 \times 10^{-5}$ emu/mol). Low-temperature data for the high-temperature phase obtained in this study have been plotted in Figure 5 along with previously obtained data[12] for the low-temperature phase.

## Results

**DSC Measurements.** The thermodynamic values obtained for the phase transitions in $(DEA)_2CuCl_4$ are $\Delta H_{tr}$ = 14.6 (9) kJ/mol and $\Delta S_{tr}$ = 45 (3) J/(mol·deg) for the thermochromic phase transition ($T_{tr}$ = 50 (1) °C) and $\Delta H_f$ = 24 (1) kJ/mol for the melting transition ($T_f$ = 83 (2) °C), in good agreement with other published results.[20] Thermodynamic data for selected DEA salts and other thermochromic copper(II) halides are collected in Table I. The values of $\Delta H_{tr}$ and $\Delta S_{tr}$ are substantially larger than those

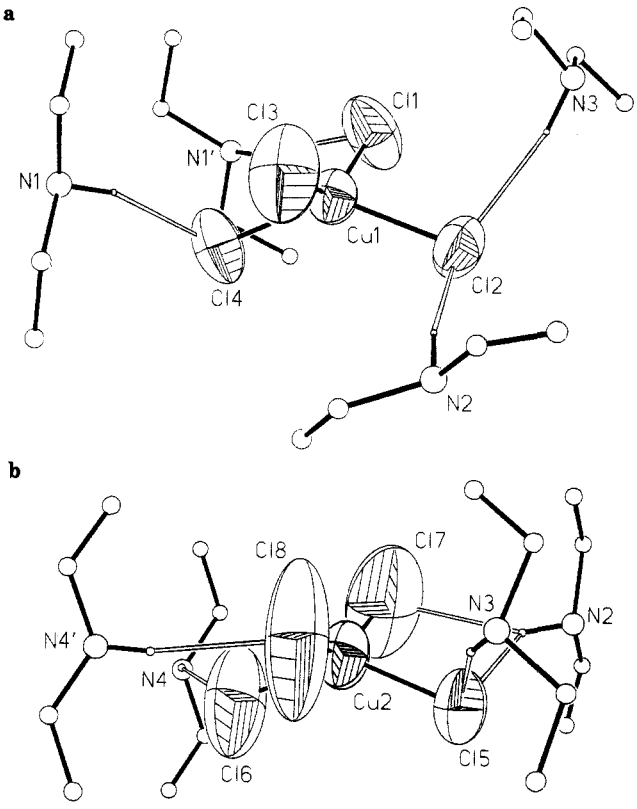


**Figure 6.** Two inequivalent anions of $[(C_2H_5)_2NH_2]_2CuCl_4$ shown with local environments (high-temperature phase). Anion ellipsoids shown at 50% probability. Cations represented by small spheres. Only the hydrogen atoms involved in the shortest N–H···Cl interactions (open lines) are included.

for other DEA salts,[19,20] e.g., $(DEA)_2ZnCl_4 \cdot xH_2O$, where the high-temperature phase involves only disorder of the DEA cations.[19] They are similar, however, to the values obtained for $[(CH_3)_2CHNH_3]_2CuCl_4$,[9] where the phase transition involves both a disordering of the organic cations and drastic rearrangement of the copper(II) chloride structure. Thus these data point to the likelihood of a gross structural rearrangement during the phase transition, rather than just a simple loss of the supercell structure observed in the green, low-temperature phase.

**Crystallography**: The structure of the yellow, high-temperature phase consists of discrete $(CuCl_4)^{2-}$ anions and DEA cations. Other than the three-dimensional ordering of ions due to inherent symmetry of the lattice, no particular ordering of ions in any favored direction is noted. Specifically, the pseudo-$S_4$ axes of the sixteen cations per unit cell are canted seemingly without bias toward any particular direction and no favored long-range one- or two-dimensional hydrogen bonding network is readily apparent. Figure 6 shows the two crystallographically inequivalent anions along with their immediate environment. The anions are oriented similarly in the figure. Both anions show similar flattened tetrahedral geometries with average trans angles of 139 (4)° and 141 (6)°; average cis angles of 97.1 (6)° and 96.2 (19)°; and average librationally uncorrected bond lengths of 2.23 (1) and 2.20 (2) Å. Again, the esd's here correspond to variations in structure rather than to experimental error. Though their geometries are similar, the two anions are distinguishable by their substantially different amplitudes of apparent motion. Both steric and hydrogen bonding effects serve to explain the notable difference between the motions of the two anions. Figure 6 shows N–H···Cl interactions with H···Cl distances less than 2.6 Å (corresponding N···Cl distances less than 3.5 Å). The shortest interaction is N(2)–H···Cl(2) = 2.281 Å (N(2)···Cl(2) = 3.224 Å). For Cu(1), the DEA cations form a partial cage around the anion, restricting its range of motion. However, for Cu(2), the cations are oriented so as to form an open-ended tube which allows an additional degree of freedom to the anion. Further, the hydrogen bonding interactions of the disordered anion form an approximately planar surface which again allows an extensive range of motion perpendicular to this two-dimensional net. The more ordered anion has hydrogen bonding interactions comprising a three-dimensional net, further restricting motion. Within each anion it is noted that the chlorine atoms with the least thermal motion, Cl(2) and Cl(5), are both involved in two hydrogen bonds. Table IV lists Cu–Cl distances both uncorrected for thermal motion and librationally corrected. The librationally corrected Cu–Cl bond lengths for Cu(2) appear to be excessively long; hydrogen bonding interactions do not explain the bond length differences between the two anions.

The four crystallographically inequivalent DEA cations are relatively fixed at their central nitrogen atoms while apparent thermal motion increases along the ethyl groups, maximizing at the terminal carbon atoms. The DEA cation containing N(1) hydrogen bonds only to the less disordered anion, and consequently it exhibits the least thermal motion of the four cations. Conversely, the cation containing N(4) hydrogen bonds only to the more disordered anion and consequently exhibits the most motion. The other two cations hydrogen bond to both anions simultaneously and so exhibit intermediate thermal motion. All four DEA cations assume an all-trans conformation. However, the unusually large amplitudes of displacement for several of the terminal $CH_3$ groups (C(5), C(12), C(13), and C(16)) indicate considerable torsional motion of the ethyl groups about the N–C bonds.

In order to further understand the relative motions of the anions of the high-temperature phase, the SHELXTL rigid-body analysis "LIBR" was extended with a local computer program "RIGBOD". This analysis allows a quantitative assessment of the intuitive feeling that a molecule or ion appears to be, for example, librating about a particular hydrogen bond. Following Shoemaker and Trueblood[21] and others,[22-24] the general motion of a rigid body may be analyzed to a quadratic degree of approximation in terms of six uncorrelated simple motions. These include three orthogonal, translational displacements plus three restricted, screw-type or helical motions along another three *nonintersecting* orthogonal axes. The analysis is simplified if the rigid molecule or ion is located on a site of symmetry within the crystal lattice so that, for example, the dynamics of a rigid molecule on an inversion center may be approximated by six motions involving three pure translational displacements and three pure librations about the point of symmetry. For the general case, analysis of the compnents of the second rank tensors defining the anisotropic thermal ellipsoids of the atoms composing the rigid body allows, at best, only 20 of the requisite 21 parameters of the motions to be determined. Thus there is some indeterminacy in the description of the motion. Another difficulty may arise from the assumption that internal vibrations of the molecule or ion are negligible in comparison with the motion of the body as a whole.[22,23] It is also assumed that the thermal ellipsoids of the molecule or ion represent a time averaging of the motion of the anions (dynamic disorder) as opposed to a lattice averaging of two or more statically occupied sites (static disorder).

Both crystallographically inequivalent $CuCl_4^{2-}$ anions of the high-temperature phase of $(DEA)_2CuCl_4$ have been analyzed in this manner as shown in Table V and Figure 7. The parameters of the motions affected by the indeterminacy mentioned above are noted in Table V and are such that constraining one parameter determines the rest. Some explanation may be useful regarding the information in Table V. The screw axes might be better referred to as fixed lines with respect to the rigid body and so are

(19) Bloomquist, D. R.; Willett, R. D. *Acta Crystallogr.* **1981**, *B37*, 1353.
(20) Van Oort, M. J. M.; Neshvad, G.; White, M. A. *J. Solid State Chem.* **1987**, *69*, 145.
(21) Schomaker, V.; Trueblood, K. N. *Acta Crystallogr.* **1968**, *B24*, 63.
(22) Johnson, C. K. *Crystallographic Computing*, Ahmed, F. R., Hall, S. R., Huber, C. P., Eds.; Munksgaard: Copenhagen, 1970; pp 209–226.
(23) Dunitz, J. D. *X-Ray Analysis and the Structure of Organic Molecules*; Cornell University Press: Ithaca and London, 1979.
(24) Sands, D. E. *Vectors and Tensors in Crystallography*; University of Kentucky, Addison-Wesley Publishing Co.: Reading, Mass., 1982.

**Table V.** Rigid-Body Analysis of the Two Crystallographically Inequivalent $CuCl_4^{2-}$ Anions in $(DEA)_2CuCl_4$ (High-Temperature Phase)

First $CuCl_4^{2-}$ Anion:

Centroid: (0.6260, 0.5219, 0.8339)
$R_w$[a] = 0.030

| | screw motion parameters | | | |
|---|---|---|---|---|
| | arbitrary point on axis | vector defining axis direction[b] | RMS librational amplitude (deg) | screw pitch (Å/deg)[c] |
| 1st axis | (0.629 (2), 0.546 (7), 0.833 (5)) | 0.0290*a* + 0.0442*b* + 0.0487*c* | 10 (2) | 0.003 (4) |
| 2nd axis | (0.636 (4), 0.543 (7), 0.780 (7)) | 0.0226*a* − 0.0789*b* + 0.0062*c* | 6.4 (5) | −0.010 (1) |
| 3rd axis | (0.659 (4), 0.522 (9), 0.846 (5)) | −0.0172*a* − 0.0290*b* + 0.0575*c* | 5.2 (4) | 0.006 (1) |

| | translational motion parameters | |
|---|---|---|
| | vector defining axis direction[b,c] | RMS translational amplitude (Å)[c] |
| 1st axis | 0.0127*a* − 0.0345*b* + 0.0696*c* | 0.290 (4) |
| 2nd axis | 0.0044*a* + 0.0885*b* + 0.0273*c* | 0.258 (5) |
| 3rd axis | 0.0383*a* + 0.0012*b* − 0.0114*c* | 0.246 (16) |

Second $CuCl_4^{2-}$ Anion

Centroid: (0.8742, 0.9529, 0.1157)
$R_w$[a] = 0.029

| | screw motion parameters | | | |
|---|---|---|---|---|
| | arbitrary point on axis | vector defining axis direction[b] | RMS librational amplitude (deg) | screw pitch (Å/deg)[c] |
| 1st axis | (0.843 (1), 0.950 (3), 0.199 (2)) | 0.0254*a* − 0.0090*b* − 0.04889*c* | 19.3 (3) | 0.0016 (3) |
| 2nd axis | (0.833 (10), 0.984 (30), 0.200 (23)) | 0.0294*a* + 0.0419*b* + 0.0496*c* | 9 (5) | −0.01 (2) |
| 3rd axis | (0.886 (42), 0.969 (37), 0.172 (84)) | 0.0117*a* − 0.0849*b* + 0.0295*c* | 4 (2) | 0.01 (1) |

| | translational motion parameters | |
|---|---|---|
| | vector defining axis direction[b,c] | RMS translational amplitude (Å)[c] |
| 1st axis | 0.0124*c* − 0.0379*b* + 0.0685*c* | 0.360 (3) |
| 2nd axis | 0.0375*a* − 0.0090*b* − 0.0147*c* | 0.295 (3) |
| 3rd axis | 0.0093*a* + 0.0866*b* + 0.0285*c* | 0.24 (10) |

[a] $R_w = [\Sigma w_{ij}(|U_{ij,o}| - |U_{ij,c}|)^2/\Sigma w_{ij}|U_{ij,o}|^2]^{1/2}$ (summed over thermal parameters of atoms defining rigid group). [b] Normalized to 1 Å. [c] Indeterminant parameter dependent upon Tr(S) constrained to equal 0. L, S, and T tensors defined elsewhere.[21,22]

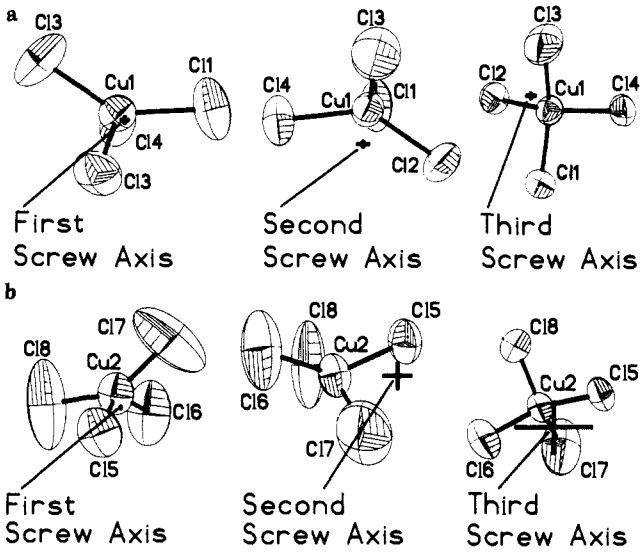


**Figure 7.** Two inequivalent anions of $[(C_2H_5)_2NH_2]_2CuCl_4$ shown at 50% probability. The three perspectives per anion are views down the three orthogonal, nonintersecting screw axes explained in the text.

each determined by a vector and a point on the axis. The translational axes on the other hand might better be called displacement vectors and so require no reference point for their definition. In Figure 7 the $CuCl_4^{2-}$ anions are pictured with the nonintersecting screw axes superimposed. Each view is oriented so that the pictured screw axis is normal to the plane of the picture; the other two nonintersecting screw axes in the plane of each picture have been removed for clarity. The two perpendicular lines in each view represent $\pm 1\sigma$ confidence limits in the true location of the screw axis.

The analysis shows that most of the motion of the anions can be ascribed to the librational components of the screw-type motions as opposed to effective translations along the screw axes (screw pitch times root-mean-square librational amplitude) or pure translations along the translational axes. From Figure 7b it is apparent that a large portion of the motion of the second $CuCl_4^{2-}$ anion involves libration approximately about the Cu(2)–Cl(5) bond, as might be expected from the hydroen bonding and steric interactions mentioned above. No rigid body analysis was completed on the cations since the large uncertainties in their anisotropic thermal parameters would propagate into unacceptably large uncertainties in their parameters of motion.

**NMR Studies.** The $^1H$ NMR signals show a pronounced decrease in line width at the phase transition temperature, indicative of a substantial increase in the thermal motion of the organic cations. The corresponding second moment of the resonance line shows a discontinuous drop of approximately 50% at that point. Above and below the transition, the line widths are nearly constant, showing only a gradual, linear decrease in width with increasing temperature of the type normally associated with the usual increase in amplitude of vibrational motions. Rather than attempting to model the $DEA^+$ motions a priori from the NMR results as was done in previous studies,[9-11] analysis will be based on deconvolution of the observed spectra into their molecular origins.

The NMR absorption spectra obtained for $(d\text{-}DEA)_2CuCl_4$ above and below the phase transition have been fit to a sum of Gaussian derivative curves by using a nonlinear least-squares program. The narrow spike at center resonance was omitted from the computer fit. Considering only nearest neighbor interactions, the contribution from the methyl protons is expected to yield a nonresolvable triplet with maximum intensity at the center of resonance and was modeled as a single Gaussian derivative with a line width of 3.82 (2) G below the phase transition and 2.53 (1) G above the transition temperature. The $CH_2$ resonance spectrum should be a resolvable doublet with maximum intensity occurring symmetrically above and below center resonance. Below the transition temperature, the $CH_2$ proton contribution was approximated as the sum of two Gaussian derivatives with a line width of 4.01 (4) G displaced 3.85 (3) G above and below center

resonance. Above the transition temperature, the pair of Gaussian derivatives are displaced ±2.50 (2) G with line widths of 3.01 (3) Gauss. The total integrated intensity of the Gaussian curves due to the $CH_2$ protons was restricted to be $^2/_3$ of that due to the methyl protons. The best computer fit for spectra of $(d\text{-DEA})_2CuCl_4$ above and below the transition are drawn as a solid line through the data points in Figure 3. The contribution to the second moment due to the ammonium protons in $(DEA)_2CuCl_4$, estimated as the difference in observed second moment for the deuteriated and nondeuteriated compound, is 3.0 $G^2$ below the transition temperature and 1.5 $G^2$ above the transition.

Although these values are only estimates, the results indicate that the 50% observed drop in the second moment at the phase transition is due to a 50% drop in the contributions of each of the three types of protons in the DEA cation. This is important in that it implies drastic weakening of the hydrogen bonding system accompanying the phase transition. If the $NH_2$ protons were strongly hydrogen bonded to the $CuCl_4^{2-}$ anions in the high-temperature phase, their contribution to the second moment would remain nearly constant through the transition. A 50% reduction in the second moment contribution can only be interpreted in terms of $NH_2$ disorder, making strong hydrogen bonding impossible.

**EPR Studies.** The single crystal and powder EPR behaviors of the low-temperature phase of $(DEA)_2CuCl_4$ have been reported at 298 and 78 K.[12] Extremely finely ground powder samples gave a typical axial Cu $d^9$ EPR spectrum, which could be interpreted to give $g_\parallel = 2.25$ and $g_\perp = 2.05$. The line width was extremely narrow and no hyperfine structure was observed. The single-crystal EPR spectrum consists of a single narrow, nearly Lorentzian line at all orientations with $\Delta H_{pp} \sim 5$ G at 78 and 15 G at room temperature. Despite the existence of three crystallographically unique $CuCl_4^{2-}$ ions only a single signal is observed. The line width and $g$ values are essentially independent of rotation about the needle axis, consistent with the fact that all the $CuCl_4^{2-}$ ions are oriented with their pseudo-$S_4$ axes parallel to the needle axis (crystallographic $a$ axis). The extremely narrow line width is due to a combination of very small dipolar broadening (resulting from the large distance between ions, 7.5 Å), coupled with the further narrowing due to the presence of the moderately strong magnetic exchange coupling (vida infra).

Figure 4 shows the temperature dependence of the EPR line widths for powder samples and single crystals of the low-temperature phase and powder samples of the high-temperature phase. All systems show a line width that increases exponentially with temperature. The line widths in the high-temperature phase are a factor of 20 times larger than those in the low-temperature phase. It is noted that the single crystal superheated by almost 20 °C, before converting to the high-temperature phase, at which point the signal was lost due to small sample size and its broad width.

Assuming that the line widths are determined by the exchange narrowing of the dipolar interaction, the large change in width would indicate a substantial decrease in the strength of the magnetic exchange coupling between the $CuCl_4^{2-}$ ion. However, the nonlinear increase in width with temperature is indicative that some other process is influencing the system giving, in particular, an indication of premonitory type behavior. While the exact mechanism is unknown, it may be due to a thermally activated rigid body motion or distortion of the $CuCl_4^{2-}$ anions, to displacement of the DEA cations weakening the hydrogen bonding (and thus the exchange coupling), or to a combination of these effects. However, since the $^1H$ NMR second moments do not exhibit any premonitory type behavior, the increased motion of the cations would appear to be an unlikely explanation.

**Magnetic Susceptibility Studies.** The low-temperature magnetic properties of the low-temperature phase of $(DEA)_2CuCl_4$ have previously been reported.[12] The weak, but significant, antiferromagnetic coupling in the system is demonstrated by the maximum observed in $\chi$ at $T \sim 5$ K. Data for the low-temperature phase are plotted as molar susceptibility versus temperature in Figure 5 with the theoretical fit described below drawn as a solid line. On the basis of the two-dimensional nature of the hydrogen-bonding scheme observed in the low-temperature structures, the magnetic susceptibility data could be fit satisfactorily to a two-dimensional Heisenberg series expansion with an antiferromagnetic exchange constant of $J/k = -1.87$ K.

The data for the quenched high-temperature phase are also plotted in Figure 5. The weaker magnetic interactions present are evidenced by the lack of a maximum in $\chi_m$ at temperatures down to 2 K. Thus, the structural rearrangement has significantly reduced the exchange coupling. This is consistent with the interpretation of the EPR results, which indicated little exchange narrowing in the high-temperature phase.

## Discussion

The thermochromic phase transition in $(DEA)_2CuCl_4$ turns out to be surprisingly complex. Structurally, the salt transforms between two monoclinic unit cells, with three independent $CuCl_4^{2-}$ anions in the low-temperature phase and two independent $CuCl_4^{2-}$ ions in the high-temperature phase. The phase transition is clearly first order in nature based on the lack of any crystallographic relationship between the two phases. No simple structural transformation pathway can be envisioned for converting one phase to the other. This accounts for the stability of the supercooled high-temperature phase as crystals of that phase, grown from the melt, can frequently be kept at room temperature for periods of several weeks.

The crystallographic study of the high-temperature phase shows the presence of disorder for both the cationic and anionic species in the structure. The magnetic resonance results further indicate that this disorder is dynamic in nature for both species. It was not possible to treat the thermal motion of the DEA cations quantitatively, but both the X-ray and NMR results indicate that the motion is quite extensive. In contrast, the motion of the $CuCl_4^{2-}$ anions was sufficiently well defined so that at least the principal contributions could be quantified. The motion of the two anions is quantitatively different. One is surrounded by four DEA cations that encage it in a manner so as to restrict its motion. The largest root-mean-square amplitude of librational motion is 10°. For the other $CuCl_4^{2-}$ anion, the four DEA cations from an open-ended tube, with hydrogen bonding such that a librational motion of 19° occurs about one axis.

The NMR line widths are essentially constant in each phase, indicating a lack of significant premonitory behavior in the motion of the DEA ions, at least on the NMR time scale. On the other hand, the EPR line widths in both phases increase very rapidly as the temperature is raised. The EPR line widths in the low-temperature phase are exchange narrowed due to the exchange coupling between $CuCl_4^{2-}$ anions through the hydrogen-bonding network. The observed strong temperature dependence in both phases implies a modulation of the hydrogen-bonding interactions on the EPR time scale. In contrast, the EPR $g$ values, indicative of the $CuCl_4^{2-}$ geometry, are essentially independent of temperature in the low-temperature phase. Thus the motion leading to the line broadening of the EPR signal must involve a temperature-dependent librational motion. The driving force for the phase transition, as with the other thermochromic salts studied, is thus entropic in nature with the increasing thermal motion of the DEA cations with increasing temperature leading to a weakening of the hydrogen bonding, allowing the eventual transformation to the more disordered high-temperature phase.

The effective weakening of the hydrogen-bonding network also allows the three independent $CuCl_4^{2-}$ anions of the low-temperature phase to relax toward the electrostatically favored tetrahedral geometry of the two independent anions of the high-temperature phase. The three anions of the low-temperature phase are geometrically dissimilar, but they are all of approximately $D_{2d}$ symmetry, whereas the two anions of the high-temperature phase are geometrically similar but deviate much more from $D_{2d}$ symmetry. These discontinuous changes in the geometry of the $CuCl_4^{2-}$ chromophore account for the thermochromic nature of the solid–solid phase transition.

The properties of this phase transition may be compared with those of the other compounds listed in Table I. For the other DEA salts, the $\Delta S_{tr}$ values are much smaller. In $(DEA)_2ZnCl_4 \cdot H_2O$

and $(DEA)_2CoCl_4$, the entropy change can be accounted for by a simple 2-fold disorder of the cation. In contrast, the $\Delta S_{tr}$ values for $(DEA)_2ZnCl_4 \cdot xH_2O$ and $(DEA)_2MnCl_4$ indicate more disorder, probably due to disorder of the ethyl groups. This is consistent with the structural results on the partially hydrated $Zn^{2+}$ salts. The three $(CH_3)_2CHNH_3^+$ salts listed are all thermochromic and their phase transitions have been investigated in some detail.[9-11] The two trihalide compounds are both linear chain compounds, and the phase transitions (the lower temperature one, in the case of the bromide) involve a rearrangement of the chain structure and the onset of a 2-fold disorder of the cation in the higher temperature phase. The $\Delta S_{tr}$ values are substantially larger than $R$ ln 2 and the excess entropy is associated with rearrangement of the chain structure. The low-temperature phase of the tetrahalide salt is a complicated chain structure involving $CuCl_4^{2-}$ anions linked by semicoordinate Cu···Cl linkages. The high-temperature phase consists of isolated distorted terahedral $CuCl_4^{2-}$ anions again with a 2-fold disorder of the cations. Again, the $\Delta S_{tr}$ value is substantially larger than the $2R$ ln 2 value. The thermal ellipsoids indicate some substantial amount of librational motion for the anions, but no detailed analysis was made. Nevertheless, the $\Delta S_{tr}$ value is not as large as that reported for $(DEA)_2CuCl_4$ in this study, in accord with the large amount of thermal motion observed for both the cations and anions. The temperature dependence of NMR line widths of the $(CH_3)_2CHNH_3^+$ salts was similar to that observed here, and the change in second moment at $T_{tr}$ could be accounted for by the observed 2-fold disorder of the cation. No unusual temperature dependence was observed for the EPR line widths either. This is in direct contrast to the observations for $(DEA)_2CuCl_4$, where the strong temperature dependence is evidence for temperature-dependent librational motion.

**Acknowledgment.** The support of PRF Grant 15813-AC6,3 is gratefully acknowledged. The X-ray facility was established through funds provided by NSF Grant CHE-8408407 and The Boeing Company.

**Supplementary Material Available:** Tables SI and SII listing thermal parameters and derived hydrogen atom positions and Figure SI giving the unit cell packing diagram (4 pages); tables of calculated and observed structure factors (20 pages). Ordering information is given on any current masthead page.

# Synthesis, Crystal Structures, Reactivity, and Magnetochemistry of a Series of Binuclear Complexes of Manganese(II), -(III), and -(IV) of Biological Relevance. The Crystal Structure of $[L'Mn^{IV}(\mu\text{-}O)_3Mn^{IV}L'](PF_6)_2 \cdot H_2O$ Containing an Unprecedented Short Mn···Mn Distance of 2.296 Å

**Karl Wieghardt,*[1a] Ursula Bossek,[1a] Bernhard Nuber,[1b] Johannes Weiss,[1b] J. Bonvoisin,[1c] M. Corbella,[1c] S. E. Vitols,[1c] and J. J. Girerd*[1c]**

*Contribution from the Lehrstuhl für Anorganische Chemie I, Ruhr-Universität, D-4630 Bochum, FRG, the Anorganisch-chemisches Institut der Universität, 6900 Heidelberg, FRG, and the Laboratoire de Spectrochimie des Elements de Transition, UA CNRS 420, Université de Paris-Sud, 91405 Orsay, France.* *Received March 15, 1988*

**Abstract:** The disproportionation reactions of two binuclear complexes of manganese(III) containing the oxo-bis(acetato)-dimanganese(III) core and two 1,4,7-triazacyclononane (L) capping ligands (**1**) or two *N,N',N''*-trimethyl-1,4,7-triazacyclononane (L') ligands (**2**) in aqueous solution under anaerobic conditions lead to a variety of novel binuclear $Mn^{III}Mn^{IV}$ and $Mn^{IV}_2$ dimers. These are the following: $[L_2Mn^{III}Mn^{IV}(\mu\text{-}O)_2(\mu\text{-}CH_3CO_2)][BPh_4]_2 \cdot CH_3CN$ (**5**); $[L'_2Mn^{III}Mn^{IV}(\mu\text{-}O)(\mu\text{-}CH_3CO_2)_2](ClO_4)_3$ (**6**); $[L_2Mn^{IV}_2(OH)_2(\mu\text{-}O)_2][Mn^{II}_3(C_2O_4)_4(OH_2)_2] \cdot 6H_2O$ (**7**); and $[L'_2Mn^{IV}_2(\mu\text{-}O)_3](PF_6)_2 \cdot H_2O$ (**9**). A tetranuclear species $[L_4Mn^{IV}_4O_6]Br_4 \cdot 5.5H_2O$ (**8**) is generated as a thermodynamically very stable product from a $Mn^{II}$ containing aqueous solution of L in the presence of oxygen. In the absence of oxygen methanolic solutions of $Mn(ClO_4)_2 \cdot 2H_2O$ or manganese(II) acetate react with L' to form $[L'_2Mn^{II}_2(\mu\text{-}OH)(\mu\text{-}CH_3CO_2)_2](ClO_4)$ (**3**) and $[L'_2Mn^{II}_2(\mu\text{-}CH_3CO_2)_3][BPh_4]$ (**4**). The oxo- and acetato-bridges in **1** and **2** are labile; addition of anions $X^-$ (X = Cl, Br, NCS, $N_3$) to acetonitrile solutions of **1** or **2** yields the monomers $LMnX_3$ and $L'MnX_3$. The electrochemistry of all compounds has been investigated; for example, **2** is reversibly oxidized by two one-electron processes to generate $Mn^{III}Mn^{IV}$ and $Mn^{IV}_2$ dimers in liquid $SO_2$. The crystal structures of **4**, **7**, **8**, and **9** have been determined by X-ray crystallography: **4**, orthorhombic *Pcab*, $a$ = 17.368 (5) Å, $b$ = 17.538 (5) Å, $c$ = 33.21 (1) Å, $Z$ = 8; **7**, monoclinic $C2/c$, $a$ = 13.391 (3) Å, $b$ = 16.571 (4) Å, $c$ = 19.312 (4) Å, $\beta$ = 109.82 (2)°, $Z$ = 4; **8**, monoclinic $P2_1/c$, $a$ = 17.548 (8) Å, $b$ = 13.118 (7) Å, $c$ = 21.56 (1) Å, $\beta$ = 105.63 (4)°, $Z$ = 4; **9**, orthorhombic *Pnma*, $a$ = 10.057 (5) Å, $b$ = 16.12 (1) Å, $c$ = 19.237 (8) Å, $Z$ = 4. **9** consists of the cofacial bioctahedral cation $(L'Mn^{IV}(\mu\text{-}O)_3Mn^{IV}L']^{2+}$ and $PF_6$ anions. The Mn···Mn distance is unusually short (2.296 (2) Å). Bulk magnetic properties of all compounds have been studied between 100 and 298 K, and in some instances 4 and 298 K. In **2** the Mn(III) ions are ferromagnetically coupled, $J$ = +18 (1) $cm^{-1}$; whereas the $Mn^{II}$ centers in **4** are weakly antiferromagnetically coupled, $J$ = −3.5 (2) $cm^{-1}$. Very strong intramolecular antiferromagnetic coupling is observed in **9** ($J$ = −780 $cm^{-1}$).

It is well established that manganese is an essential trace element in biology.[2] The oxidation of water by photosynthetic enzymes (photosystem II; PS II),[3] the reduction of ribonucleotides in certain bacteria,[4] and the disproportionation of hydrogen

0002-7863/88/1510-7398$01.50/0 